Molecular Vision 2024; 30:268-277 <http://www.molvis.org/molvis/v30/268>
Received 3 June 2023 | Accepted 1 July 2024 | Published 2 July 2024

Complement C3 is downregulated following ranibizumab intervention in experimental central retinal vein occlusion

Lasse Jørgensen Cehofski,[1,2,3] Anders Kruse,[4] Mads Odgaard Mæng,[4] Benedict Kjaergaard,[2] Benn Falch Sejergaard,[4] Anders Schlosser,[5] Grith Lykke Sorensen,[5] Bent Honoré,[6,7] Henrik Vorum[4,7]

[1]Department of Ophthalmology, Odense University Hospital, Odense, Denmark; [2]Biomedical Research Laboratory, Aalborg University Hospital, Aalborg, Denmark; [3]Department of Clinical Research, University of Southern Denmark, Odense, Denmark; [4]Department of Ophthalmology, Aalborg University Hospital, Aalborg, Denmark; [5]Department of Cancer and Inflammation Research, Institute for Molecular Medicine, University of Southern Denmark, Odense, Denmark; [6]Department of Biomedicine, Aarhus University, Aarhus, Denmark; [7]Department of Clinical Medicine, Aalborg University, Aalborg University Hospital

Purpose: Ranibizumab is a frequently used inhibitor of vascular endothelial growth factor (VEGF) in the treatment of macular edema following central retinal vein occlusion (CRVO). Studying proteins that mediate the beneficial effects of ranibizumab in CRVO can potentially lead to the improved management of macular edema.
Methods: In 14 Danish Landrace pigs, experimental CRVO was induced in the right eyes and treated with either intravitreal ranibizumab (n = 6) or an intravitreal sodium chloride 9 mg/mL solution as a sham injection (n = 8). Successful CRVO was confirmed by fluorescein angiography. Retinal samples were collected 15 days after induced CRVO and analyzed with label-free, quantification, nano-liquid chromatography–tandem mass spectrometry. Validation was performed with western blotting and immunohistochemistry.
Results: CRVO was successfully induced and confirmed by fluorescein angiography. A total of 28 proteins were upregulated, and 31 proteins were downregulated following ranibizumab treatment. A high concentration of the ranibizumab component immunoglobulin kappa chain C region was observed in retinas treated with ranibizumab. Complement C3, the Ig lambda chain C region, and nucleobindin-2 were downregulated following ranibizumab intervention. The downregulation of complement C3 was confirmed by western blotting. Modest changes were observed in the remaining significantly regulated proteins.
Conclusions: Retinal complement C3 was downregulated following ranibizumab intervention in CRVO. The decrease in complement C3 may potentially downregulate the inflammatory response in CRVO. A high retinal concentration of ranibizumab was reached 15 days after injection of the compound.

Central retinal vein occlusion (CRVO) is a visually disabling condition resulting from impaired outflow of the central retinal vein, the major outflow vessel of the eye [1,2]. The visual outcome in CRVO can be devastating, and blindness may be the ultimate result. Visual impairment in CRVO is predominantly caused by macular edema and visual acuity rarely improves above 20/40 if treatment is not initiated [3-6].

Macular edema in CRVO arises through a complex multifactorial mechanism. Occlusion of the central retinal vein increases the resistance to blood flow in retinal arterioles with closure of retinal capillaries and small arterioles, leading to retinal hypoxia. Retinal hypoxia results in increased production of vascular endothelial growth factor A (VEGF-A) and a complex inflammatory response mediated by interleukin (IL)-6, IL-8, IL-18, S100A12, fibrinogen, fibronectin, galectin-3, and monocyte chemotactic protein-1 [7-11], which increases vascular permeability and leads to the accumulation of fluid in the macula [8]. In retinal vein occlusion, intraocular complement factors have recently been found to correlate with visual acuity and the severity of macular edema, indicating involvement in pathological processes leading to visual loss [10,11].

Macular edema is effectively treated with intravitreal anti-VEGF injections as a first-line therapy, while dexamethasone intravitreal implants are considered second-line treatments [12-15]. Despite significant therapeutic advances, CRVO remains a burden to patients and continues to challenge clinicians, as well as the healthcare system in general. Macular edema is recurrent in most cases, and approximately 50% of patients need anti-VEGF injections four years after being diagnosed with either CRVO or branch retinal vein occlusion (BRVO) [16].

Ranibizumab is a monoclonal antibody fragment (Fab) that neutralizes all isoforms of VEGF-A [17]. Studying protein changes downstream of VEGF-A neutralization by ranibizumab may elucidate novel mechanisms that mediate

Correspondence to: Lasse Jørgensen Cehofski, Department of Ophthalmology, Odense University Hospital Sdr. Boulevard 29, 5000 Odense, Denmark; Phone +45 53558878; email: lassecehofski@hotmail.com

the beneficial response to anti-VEGF treatment. The retinal proteome in CRVO following ranibizumab treatment has not previously been explored. Here, we report on retinal proteome changes following ranibizumab intervention in an experimental model of CRVO.

METHODS

Animal preparation: The study was approved by the Danish Animal Experiments Inspectorate, permission no. 2019–15–0201- 01651, and the experiments were conducted in accordance with the guidelines published by the Institute for Laboratory Animal Research. A total of 14 Danish Landrace pigs were used for the experiments and housed under a 12-h light/dark cycle. General anesthesia, topical anesthesia with eye drops, and dilation of the pupils were performed as previously described [18].

Experimental central retinal vein occlusion (CRVO): Experimental CRVO was induced in proximity to the optic nerve head with a standard argon laser (532 nm), given by indirect ophthalmoscopy using a 20D lens. The laser energy was set to 400 mW, with an exposure time of 550 ms. A total of 30–40 laser applications were used per occlusion. By applying the laser directly to the retinal veins close to the optic nerve head, the thrombotic material was directed toward the optic nerve head and lamina cribrosa. Experimental CRVO was considered successful when stagnation of venous blood and the development of flame-shaped hemorrhages were observed by indirect ophthalmoscopy. In the intervention group, the right eye of the animal (n = 6) received an intravitreal injection of 0.05 ml ranibizumab 10 mg/ml (Novartis A/S, Copenhagen, Denmark). In the control group, the right eye of each animal (n = 8) received a vehicle injection with 0.05 ml of sodium chloride 9 mg/ml (NaCl; B. Braun, Denmark).

Fifteen days after induced CRVO, the eyes were enucleated and dissected on ice under a microscope. The animals were euthanized immediately after enucleation. The anterior segment was removed, and the vitreous body was removed by aspiration into a 5 ml syringe. In eyes used for proteomic analysis, the neurosensory retina was peeled from the retinal pigment epithelium/choroid complex with tweezers and stored at -80 °C. In eyes collected for immunohistochemistry, complexes consisting of the neurosensory retina, RPE/choroid complex, and sclera were excised.

Sample preparation for mass spectrometry: Label-free, quantification, nano-liquid chromatography–tandem mass spectrometry (LFQ nLC-MS/MS) was performed to compare CRVO + ranibizumab (n = 5) and CRVO + NaCl (n = 7). Sample preparation was undertaken, as previously described [19]. Briefly, lysis with a buffer of 5% sodium deoxycholate and 20 mM triethyl ammonium bicarbonate was performed, as previously described [20]. The protein concentration was measured by infrared spectrometry with a Direct Detect Spectrometer (Merck KGaA, Darmstadt, Germany), and alkylation with iodoacetamide was performed, as previously described [19]. The resulting lysates were added to filter units (Microcon Centrifugal Filter Devices 30 K, MilliporeSigma, Sigma Aldrich, Søborg, Denmark), and digestion with trypsin was performed using S-Trap micro spin columns from Protifi (Hintington, NY), as described previously [10]. Finally, the samples were dried in a vacuum centrifuge and resuspended in 100 mM etraethylammonium bromide, followed by measurement of the peptide concentration by fluorescence, as previously described [20]. Peptides were dried and dissolved in 1% formic acid, and 1 µg was injected into the mass spectrometer.

Label-free, quantification, nano-liquid chromatography–tandem mass spectrometry (LFQ nLC-MS/MS): LFQ nLC-MS/MS was performed on an Orbitrap Fusion Tribrid mass spectrometer equipped with an EasySpray ion source coupled to a Dionex Ultimate™ 3000 RSLC nanosystem (Thermo Fisher Scientific Instruments, Waltham, MA) using the Universal Method for label-free quantification, as previously described [10,15]. Peptide separation was performed, as previously described [19]. Mass spectrometry was performed with the Universal Method for label-free quantification, and full scans in the Orbitrap were obtained, as previously described [19]. Isolation of precursor ions in the quadrupole, collision-induced dissociation, and detection of MS^2 scans in the ion trap were performed, as previously described [19]. MaxQuant software version 1.6.6.0 [21] (Max Planck Institute of Biochemistry, Martinsried, Germany) was used to search raw data files against the Uniprot *Sus scrofa* and *Homo sapiens* databases.

Filtration of proteins and statistics: Unfiltered MaxQuant output files (Appendix 1) were uploaded to Perseus software version 1.6.2.3 [22] (Max Planck Institute of Biochemistry, Martinsried, Germany). Proteins were filtrated by removal of proteins only identified by the modification site, followed by removal of proteins identified from a peptide that was found to be part of a protein derived from the reversed part of the decoy database. Proteins identified as contaminants were also removed from the dataset. Quantitative values were log2 transformed, and technical replicates were averaged. Successful identification of a protein requires at least two unique peptides. Successful identification and quantification were required in 100% of the samples. A Student's *t*-test was performed in Perseus to compare CRVO + ranibizumab (n

= 5) versus CRVO + NaCl (n = 7). Proteins were considered significantly regulated if $p < 0.05$ by Student *t* test.

Immunohistochemistry: Eyes from one animal were used to compare CRVO + ranibizumab (n = 1) versus CRVO + NaCl (n = 1). Complexes consisting of the retina, choroid, and sclera were fixated in formalin for 24 h, followed by removal of the formalin solution. The tissue was then stored in a PBS solution at 4°C until further use. Immunohistochemistry was performed as previously described [23] with a rabbit anti-pig complement component 3 antibody (MBS2028490, MyBiosource, San Diego, CA), diluted 1:100.

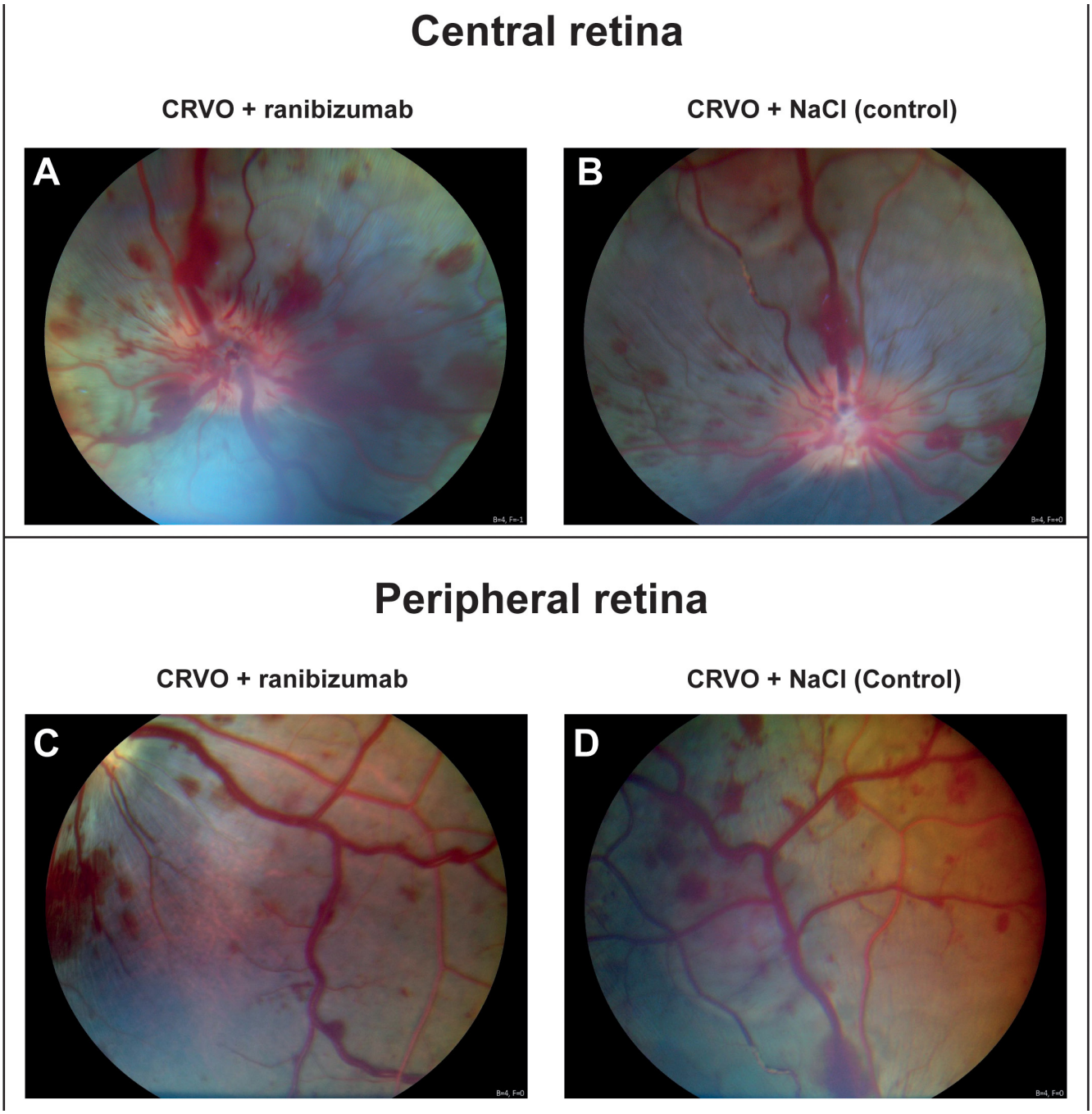

Figure 1. Fluorescein angiography of experimental CRVO. **A**–**B**: Venous tortuosity and dilation, and flame-shaped hemorrhages appearing within 30 min after induced CRVO. Experimental CRVO was treated with either ranibizumab or NaCl (control). **C**–**D**: Flame-shaped hemorrhages in the peripheral retina following experimental CRVO.

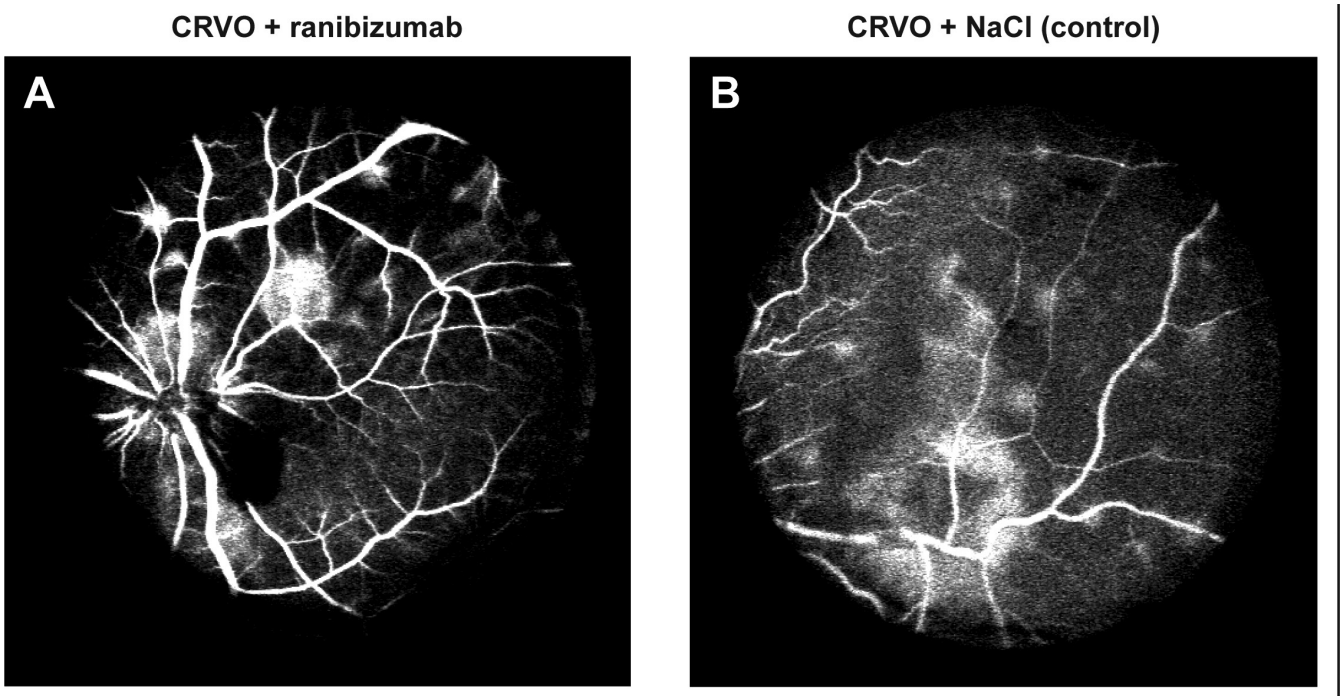

Figure 2. Fluorescein angiography was performed four days after CRVO was induced. **A** and **B**: Venous tortuosity and leakage of fluorescein were observed in all four quadrants, consistent with successfully induced CRVO. Fluorescein angiography was shown for one eye treated with ranibizumab and one eye treated with NaCl.

Western blotting: Western blotting was performed as previously described [23] using a polyclonal rabbit anti-pig complement component 3 antibody (MBS2028490, MyBioSource, San Diego, CA), diluted 1:1,000. Western blotting was performed to compare CRVO + ranibizumab (n = 5) versus CRVO + NaCl (n = 7). Statistical analysis of densitometric data was performed with the Mann–Whitney U test.

RESULTS

Retinal proteome changes following ranibizumab intervention in experimental CRVO: Experimental CRVO was successfully induced in all eyes. Venous tortuosity and flame-shaped hemorrhages were observed in all animals within 30 min after CRVO was induced (Figure 1). Venous tortuosity, leakage, and areas with retinal capillary nonperfusion were observed on angiography in all quadrants, consistent with successfully induced CRVO (Figure 2).

In total, 2,342 proteins were successfully identified. All successfully identified proteins are provided in Appendix 2. A total of 1,518 proteins were successfully identified and quantified in 100% of the samples (Appendix 3). Statistical analysis was performed on the proteins present in 100% of the samples. A total of 59 proteins were significantly regulated in the ranibizumab intervention in CRVO (Figure 3; Table 1). A total of 28 proteins were upregulated, and 31 proteins were downregulated. The largest upregulation was observed in the Ig kappa chain C region, a component of ranibizumab. Other upregulated proteins included the tubulin beta-6 chain (fold change = 2.2; p = 0.031) and the very-long-chain (3R)-3-hydroxyacyl-CoA dehydratase 3 (fold change = 1.66; p = 0.018; Table 1). The remaining upregulated proteins had fold changes between 1.07 and 1.36. Downregulated proteins included complement C3 (fold change = 0.44; p = 0.039), the Ig lambda chain C region (fold change = 0.47; p = 0.049), nucleobindin-2 (fold change = 0.64; p = 0.008), transthyretin (fold change = 0.67; p = 0.037), prolow-density lipoprotein receptor-related protein 1 (fold change = 0.68; p = 0.048), and 14 kDa phosphohistidine phosphatase (fold change = 0.68; p = 0.020; Table 1). All other downregulated proteins had fold changes between 0.68 and 0.95; western blotting confirmed a decreased level of complement C3 following ranibizumab intervention (p = 0.048; Figure 4). Complement C3 was predominantly expressed in the retinal nerve fiber layer, inner plexiform layer, outer plexiform layer, and outer nuclear layer (Figure 5).

DISCUSSION

Our study reported on proteome changes in an experimental model of CRVO. As the majority of CRVO cases are nonischemic [2], a CRVO model corresponding to nonischemic CRVO was chosen for the study. Leakage of fluorescein along retinal veins, as well as areas with retinal capillary nonperfusion, were observed on fluorescein angiography consistent with angiographic findings following CRVO in humans. Alternatively, an ischemic CRVO can be created by occluding four branch retinal veins in the porcine eye, but stages with severe ischemia may be more resistant to anti-VEGF therapy [24]. The experimental CRVO model was discussed in detail in a recent paper [25]. The model has several advantages that make it suitable for proteome studies of retinal vascular diseases. The porcine retina is fully vascularized and similar to the human retina in size and photoreceptor distribution [25,26]. Significant drawbacks associated with the use of porcine eyes include the high expenses related to acquisition and housing, which generally make it necessary to conduct experiments with small sample sizes.

Proteomic analysis identified downregulation of retinal complement C3 in eyes treated with ranibizumab. The quantitative validation of the mass spectrometry data was performed by western blotting. Complement C3 was found to be increased in aqueous humor samples from patients with CRVO [11] and BRVO [10]. In aqueous humor from patients with BRVO, a correlation between complement C3 and the severity of macular edema has previously been identified [10]. At the retinal level, complement C3 is increased in experimental CRVO, where it increases with the level of retinal ischemia [9,23]. Interestingly, our study observed a reversal of complement C3 in retinas treated with ranibizumab.

The complement system is part of the innate immune response, the fast, unspecific arm of the immune system, and it is involved in the early response against pathogens [27,28]. The complement system can be activated through three different pathways: the classical pathway, the lectin pathway, and the alternative pathway [27].

The alternative pathway is constitutively active at low levels due to the spontaneous hydrolysis of complement

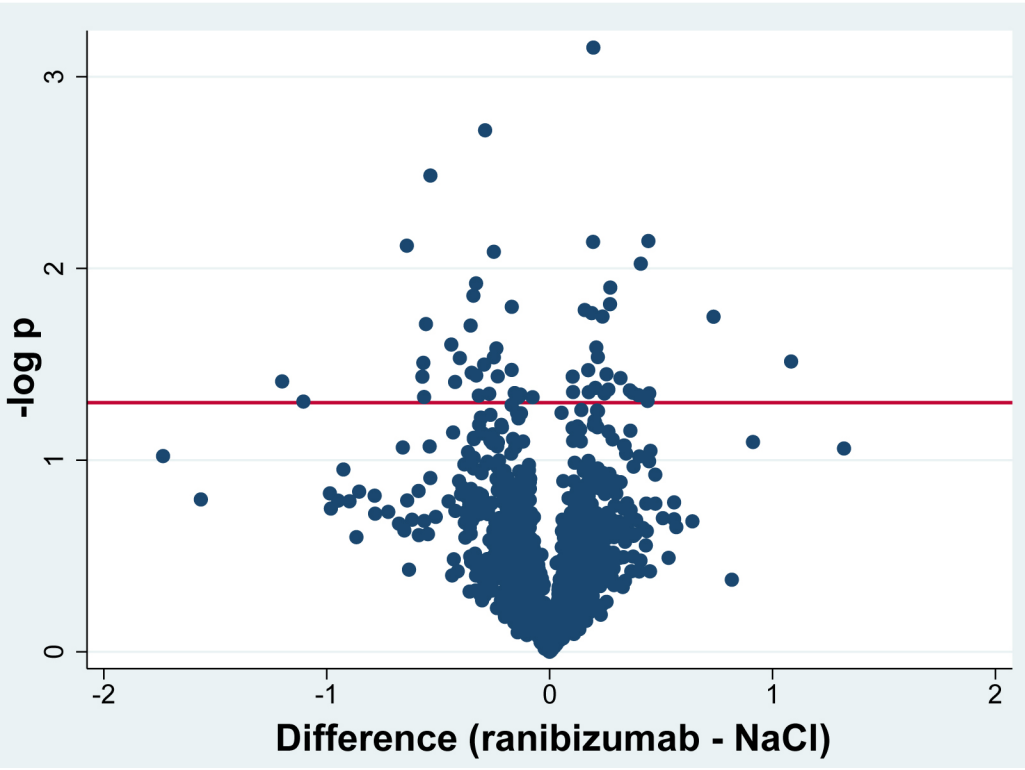

Figure 3. Volcano plot. The log2-transformed abundance ratio (ranibizumab/NaCl) for each protein is plotted on the x-axis. Negative log10 transformed p values from the Student t-test are plotted on the y-axis. Statistically significantly regulated proteins are located above the horizontal line, which denotes a significance level of 0.05. The components of ranibizumab are not included in the volcano plot.

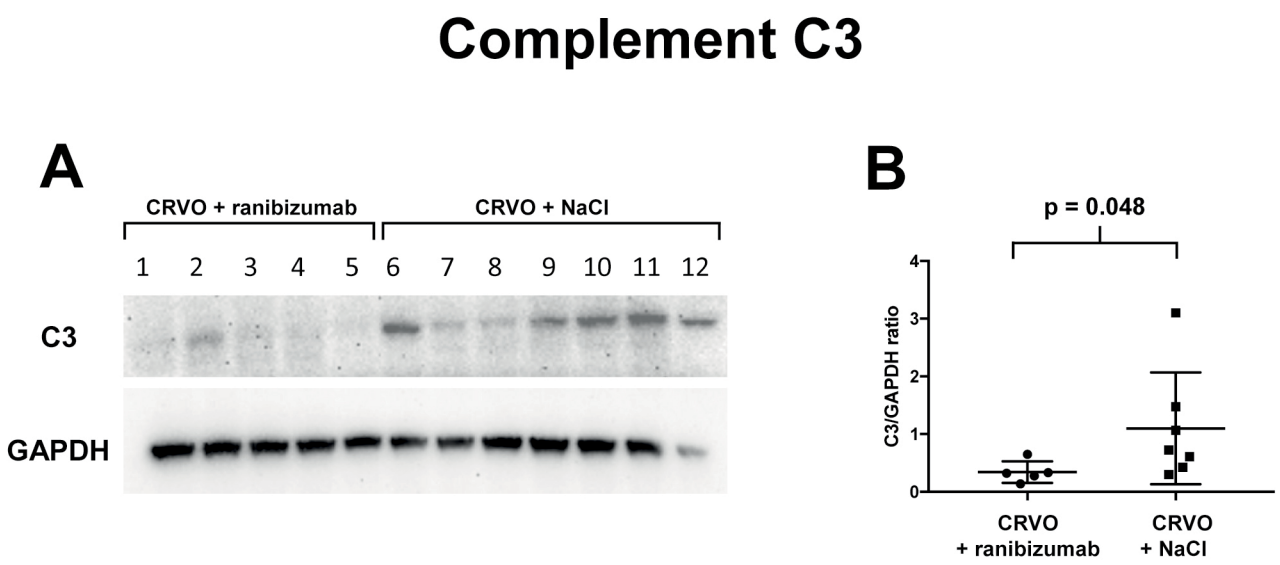

Figure 4. Western blotting. **A**: Western blotting comparing complement C3 in CRVO + ranibizumab (lanes 1–5) versus CRVO + NaCl (lanes 6–12). **B**: Densitometric data corresponding to (A) confirmed downregulation of complement C3 (p = 0.048).

component C3 to C3(H_2O). In the alternative pathway, factor B can bind C3(H_20) and is cleaved by factor D to form a distinct C3 convertase termed C3(H_20), which produces C3b and provides an amplification loop for the activation of the complement system [28]. There is mounting evidence that the complement system plays an important role in the pathogenesis of age-related macular degeneration [29]. Interestingly, a bispecific fusion protein that neutralizes VEGF along with complement C3b and complement C4b has shown promising results in animal models of neovascular age related macular degeneration and has been reported to be well tolerated in a phase 1 trial [29]. Genotyping of patients with neovascular AMD has identified an association between these complements.

Furthermore, the C3 gene has been associated with favorable outcomes of anti-VEGF therapy. There is still limited

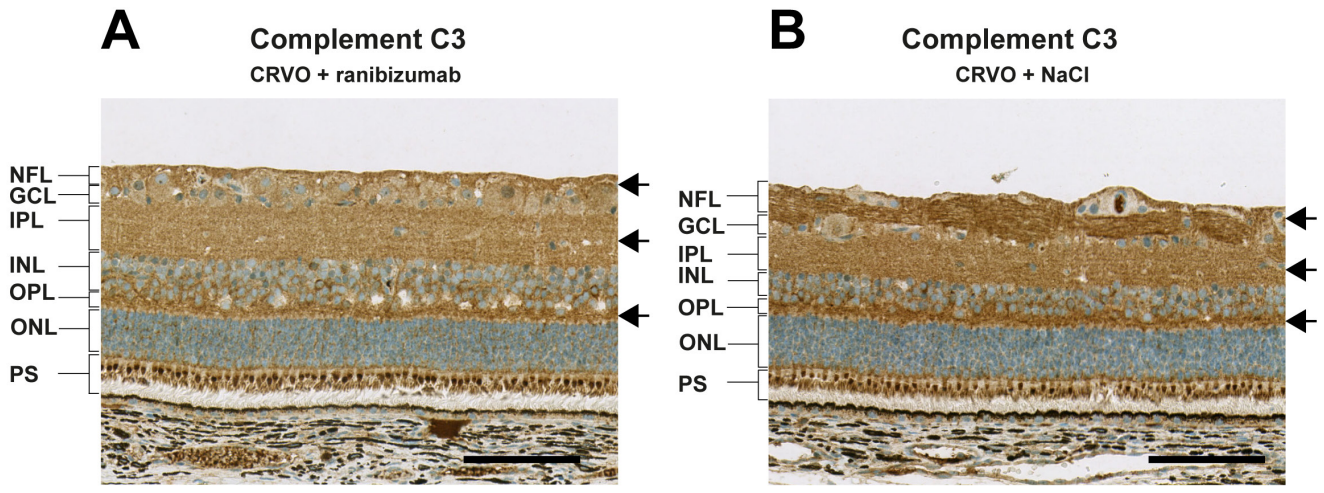

Figure 5. Immunohistochemistry. **A** and **B**: Complement C3 was predominantly expressed in the retinal nerve fiber layer, inner plexiform layer, outer plexiform layer, and outer nuclear layer (Scale bar = 100 µm). Reaction color: Brown. Abbreviations: NFL: nerve fiber layer; GCL: ganglion cell layer; IPL: inner plexiform layer; INL: inner nuclear layer; OPL: outer plexiform layer; ONL: outer nuclear layer; PS: photoreceptor segments.

Table 1. Significantly regulated proteins ordered according to fold change.

Protein ID	Protein name	Gene	P-value	Fold change
P01834	Ig kappa chain C region	IGKC	2×10^{-7}	12.2
Q9BUF5	Tubulin beta-6 chain	TUBB6	0.031	2.12
Q9P035	Very-long-chain (3R)-3-hydroxyacyl-CoA dehydratase 3	HACD3	0.018	1.66
Q16518	Retinoid isomerohydrolase	RPE65	0.045	1.36
Q9H2P0	Activity-dependent neuroprotector homeobox protein	ADNP	0.007	1.36
Q9BTT0-3	Acidic leucine-rich nuclear phosphoprotein 32 family member E	ANP32E	0.049	1.36
O14639-2	Actin-binding LIM protein 1	ABLIM1	0.009	1.33
Q92530	Proteasome inhibitor PI31 subunit	PSMF1	0.046	1.32
O02772	Fatty acid-binding protein. heart	FABP3	0.045	1.29
Q9TUI8	Fatty-acid amide hydrolase 1	FAAH	0.043	1.28
P25685	DnaJ homolog subfamily B member 1	DNAJB1	0.037	1.25
Q8ND76-3	Cyclin-Y	CCNY	0.013	1.21
P41223	Protein BUD31 homolog	BUD31	0.015	1.21
Q92598-2	Heat shock protein 105 kDa	HSPH1	0.043	1.2
Q04917	14-3-3 protein eta	YWHAH	0.036	1.19
P11137-3	Microtubule-associated protein 2	MAP2	0.045	1.19
O14787-2	Transportin-2	TNPO2	0.018	1.18
Q12931-2	Heat shock protein 75 kDa, mitochondrial	TRAP1	0.029	1.16
Q5JPE7-2	Nodal modulator 2	NOMO2	0.026	1.16
Q14847	LIM and SH3 domain protein 1	LASP1	0.042	1.15
Q14498-3	RNA-binding protein 39	RBM39	7×10^{-4}	1.15
Q12756	Kinesin-like protein KIF1A	KIF1A	0.007	1.14
Q16543	Hsp90 co-chaperone Cdc37	CDC37	0.017	1.14
F1SPM8	AP2-associated protein kinase 1	AAK1	0.044	1.13
Q92990-2	Glomulin	GLMN	0.034	1.13
Q99497	Protein deglycase DJ-1	PARK7	0.016	1.12
P78371	T-complex protein 1 subunit beta	CCT2	0.044	1.08
Q93009	Ubiquitin carboxyl-terminal hydrolase 7	USP7	0.037	1.07
Q16531	DNA damage-binding protein 1	DDB1	0.047	0.95
Q9BPX5	Actin-related protein 2/3 complex subunit 5-like protein	ARPC5L	0.045	0.91
P43367	Calpain-2 catalytic subunit	CAPN2	0.046	0.91
Q99816	Tumor susceptibility gene 101 protein	TSG101	0.047	0.91
O43264	Centromere/kinetochore protein zw10 homolog	ZW10	0.045	0.9
Q2YGT9	60S ribosomal protein L6	RPL6	0.016	0.89
O00629	Importin subunit alpha-3	KPNA4	0.034	0.89
P60983	Glia maturation factor beta	GMFB	0.037	0.85
O75436	Vacuolar protein sorting-associated protein 26A	VPS26A	0.026	0.85
P61313	60S ribosomal protein L15	RPL15	0.029	0.84
P41227-2	N-alpha-acetyltransferase 10	NAA10	0.008	0.84
Q6QAP7	40S ribosomal protein S17	RPS17	0.045	0.83
P27708	CAD protein	CAD	0.002	0.82

Protein ID	Protein name	Gene	P-value	Fold change
P62495-2	Eukaryotic peptide chain release factor subunit 1	ETF1	0.032	0.82
P36404	ADP-ribosylation factor-like protein 2	ARL2	0.046	0.8
P61586	Transforming protein RhoA	RHOA	0.036	0.8
P36887	cAMP-dependent protein kinase catalytic subunit alpha	PRKACA	0.012	0.8
P52294	Importin subunit alpha-5	KPNA1	0.014	0.79
O15240	Neurosecretory protein VGF	VGF	0.035	0.78
P61964	WD repeat-containing protein 5	WDR5	0.02	0.78
P12026	Acyl-CoA-binding protein	DBI	0.029	0.76
P52209-2	6-phosphogluconate dehydrogenase. decarboxylating	PGD	0.039	0.75
O60502	Protein O-GlcNAcase	MGEA5	0.025	0.74
P15145	Aminopeptidase N	ANPEP	0.003	0.69
P59083	14 kDa phosphohistidine phosphatase	PHPT1	0.02	0.68
Q07954	Prolow-density lipoprotein receptor-related protein 1	LRP1	0.047	0.68
P80895	Protein-L-isoaspartate(D-aspartate) O-methyltransferase	PCMT1	0.031	0.68
P50390	Transthyretin	TTR	0.037	0.67
P80303-2	Nucleobindin-2	NUCB2	0.008	0.64
P01846	Ig lambda chain C region	n/a	0.049	0.47
P01025	Complement C3	C3	0.039	0.44

knowledge of the role of complement activation in CRVO, but our data suggest that ranibizumab may downregulate the inflammatory response in CRVO by decreasing the expression of complement C3.

Ranibizumab intervention was associated with a decreased level of nucleobindin-2, a protein with two Ca^{2+} binding EF-hand domains separated by an acidic amino acid-rich region and a leucine zipper [30]. The heterogenic structure of nucleobindin-2 is consistent with its multitude of functions. In a variety of cancers, nucleobindin-2 promotes cell proliferation, migration, and invasion, with high nucleobindin-2 levels associated with poor outcomes [30,31], but its retinal function remains to be elucidated. A downregulation of transthyretin was observed following ranibizumab intervention. Ocular transthyretin is synthesized by RPE cells and has a wide distribution within the retinal layers [32,33], but the role of transthyretin in the RPE remains to be elucidated [31]. The immunoglobulin kappa chain C region of ranibizumab was identified in samples treated with ranibizumab, reflecting high retinal concentrations of the compound 15 days after the intervention. The porcine protein Ig lambda chain C region was downregulated following ranibizumab intervention. The downregulation of the porcine Ig lambda chain C region is likely to result from a restored blood–retinal barrier after anti-VEGF therapy [26].

While proteomics allows for the identification and quantification of a large set of proteins, the approach has several limitations. In particular, the quantification of low-abundance proteins is a significant challenge in proteomics. VEGF, a well-known, low-abundance protein, was not identified in the proteomic analysis in our study. Several factors contribute to difficulties in detecting low-abundance proteins [10,11]. These include sample complexity, technical variation, and fragmentation efficiency. Furthermore, the complexity of the retina, with its multilayered structure and multiple cell types, contributes to the complexity of the tissue, which can make it difficult to detect VEGF [24].

Conclusion: Our study identified downregulation of complement C3 in CRVO treated with ranibizumab. Ranibizumab intervention may potentially contribute to downregulation of the inflammatory response in CRVO by decreasing the retinal level of complement C3. Ranibizumab intervention was also associated with downregulation of the Ig lambda chain C region, which may reflect the reestablishment of the blood–retinal barrier with decreased leakage of plasma proteins. A high concentration of the ranibizumab component Ig kappa chain C region was detected, reflecting high levels of ranibizumab reached in the retina 15 days after injection.

APPENDIX 1. SUPPLEMENTARY TABLE 1.

To access the data, click or select the words “Appendix 1.”

APPENDIX 2. SUPPLEMENTARY TABLE 2.

To access the data, click or select the words "Appendix 2."

APPENDIX 3. SUPPLEMENTARY TABLE 3.

To access the data, click or select the words "Appendix 3."

FINANCIAL SUPPORT

The study was funded by Fight for Sight Denmark, Helene og Viggo Bruuns Fond, the Svend Andersen Foundation, the Bagger-Sørensen Foundation, the Obel Family Foundation, the Herta Christensen Foundation, the North Denmark Region (2013–0076797), Overlægerådets Forskningsfond at Odense University Hospital, and Speciallæge Heinrich Kopps Legat. The mass spectrometers used for the present study were funded by A.P. Møller og Hustru Chastine Mc-Kinney Møllers Fond til almene Formaal.

REFERENCES

1. Green WR, Chan CC, Hutchins GM, Terry JM. Central retinal vein occlusion: a prospective histopathologic study of 29 eyes in 28 cases. Trans Am Ophthalmol Soc 1981; 79:371-422. [PMID: 7342407].
2. Hayreh SS, Podhajsky PA, Zimmerman MB. Natural history of visual outcome in central retinal vein occlusion. Ophthalmology 2011; 118:119-133.e1. , 2. [PMID: 20723991].
3. Hayreh SS, Zimmerman MB. Branch retinal vein occlusion: natural history of visual outcome. JAMA Ophthalmol 2014; 132:13-22. [PMID: 24158729].
4. Rehak J, Rehak M. Branch retinal vein occlusion: pathogenesis, visual prognosis, and treatment modalities. Curr Eye Res 2008; 33:111-31. [PMID: 18293182].
5. Newman-Casey PA, Stem M, Talwar N, Musch DC, Besirli CG, Stein JD. Risk factors associated with developing branch retinal vein occlusion among enrollees in a United States managed care plan. Ophthalmology 2014; 121:1939-48. [PMID: 24953793].
6. McIntosh RL, Rogers SL, Lim L, Cheung N, Wang JJ, Mitchell P, Kowalski JW, Nguyen HP, Wong TY. Natural history of central retinal vein occlusion: an evidence-based systematic review. Ophthalmology 2010; 117:1113-1123.e15. [PMID: 20430446].
7. Noma H, Mimura T, Yasuda K, Shimura M. Role of soluble vascular endothelial growth factor receptor signaling and other factors or cytokines in central retinal vein occlusion with macular edema. Invest Ophthalmol Vis Sci 2015; 56:1122-8. [PMID: 25634982].
8. Campochiaro PA, Akhlaq A. Sustained suppression of VEGF for treatment of retinal/choroidal vascular diseases. Prog Retin Eye Res 2021; 83:100921[PMID: 33248215].
9. Cehofski LJ, Kruse A, Kirkeby S, Alsing AN, Ellegaard Nielsen J, Kojima K, Honoré B, Vorum H. IL-18 and S100A12 Are Upregulated in Experimental Central Retinal Vein Occlusion. Int J Mol Sci 2018; 19:3328-[PMID: 30366444].
10. Cehofski LJ, Kojima K, Terao N, Kitazawa K, Thineshkumar S, Grauslund J, Vorum H, Honoré B. Aqueous Fibronectin Correlates With Severity of Macular Edema and Visual Acuity in Patients With Branch Retinal Vein Occlusion: A Proteome Study. Invest Ophthalmol Vis Sci 2020; 61:6-[PMID: 33270842].
11. Cehofski LJ, Kojima K, Kusada N, Rasmussen M, Muttuvelu DV, Grauslund J, Vorum H, Honoré B. Macular Edema in Central Retinal Vein Occlusion Correlates With Aqueous Fibrinogen Alpha Chain. Invest Ophthalmol Vis Sci 2023; 64:23-[PMID: 36820679].
12. Haller JA, Bandello F, Belfort R Jr, Blumenkranz MS, Gillies M, Heier J, Loewenstein A, Yoon YH, Jiao J, Li XY, Whitcup SM, Li J. Ozurdex GENEVA Study Group. Dexamethasone intravitreal implant in patients with macular edema related to branch or central retinal vein occlusion twelve-month study results. Ophthalmology 2011; 118:2453-60. [PMID: 21764136].
13. Cehofski LJ, Kruse A, Magnusdottir SO, Alsing AN, Nielsen JE, Kirkeby S, Honoré B, Vorum H. Dexamethasone intravitreal implant downregulates PDGFR-α and upregulates caveolin-1 in experimental branch retinal vein occlusion. Exp Eye Res 2018; 171:174-82. [PMID: 29505751].
14. Higham A, Jacob S, Cox M, Baker C, Al-Husainy S, Sivaraj R, Gibson JM. The efficacy and safety of intravitreal dexamethasone implants for macular oedema secondary to retinal vein occlusion: 3-year experience. Acta Ophthalmol 2016; 94:e674-5. [PMID: 27010078].
15. Cehofski LJ, Kruse A, Mæng MO, Sejergaard BF, Schlosser A, Sorensen GL, Grauslund J, Honoré B, Vorum H. Dexamethasone Intravitreal Implant Is Active at the Molecular Level Eight Weeks after Implantation in Experimental Central Retinal Vein Occlusion. Molecules 2022; 27:5687-[PMID: 36080454].
16. Campochiaro PA, Sophie R, Pearlman J, Brown DM, Boyer DS, Heier JS, Marcus DM, Feiner L, Patel A. RETAIN Study Group. Long-term outcomes in patients with retinal vein occlusion treated with ranibizumab: the RETAIN study. Ophthalmology 2014; 121:209-19. [PMID: 24112944].
17. Papadopoulos N, Martin J, Ruan Q, Rafique A, Rosconi MP, Shi E, Pyles EA, Yancopoulos GD, Stahl N, Wiegand SJ. Binding and neutralization of vascular endothelial growth factor (VEGF) and related ligands by VEGF Trap, ranibizumab and bevacizumab. Angiogenesis 2012; 15:171-85. [PMID: 22302382].
18. Cehofski LJ, Kruse A, Kjærgaard B, Stensballe A, Honoré B, Vorum H. Proteins involved in focal adhesion signaling pathways are differentially regulated in experimental branch retinal vein occlusion. Exp Eye Res 2015; 138:87-95. [PMID: 26086079].

19. Cehofski LJ, Kruse A, Alsing AN, Sejergaard BF, Nielsen JE, Pedersen S, Muttuvelu DV, Kirkeby S, Honoré B, Vorum H. Aflibercept Intervention in Experimental Branch Retinal Vein Occlusion Results in Upregulation of DnaJ Homolog Subfamily C Member 17. J Ophthalmol 2021; 2021:6690260[PMID: 33747556].

20. Honoré B. Proteomic Protocols for Differential Protein Expression Analyses. Methods Mol Biol 2020; 2110:47-58. [PMID: 32002900].

21. Tyanova S, Temu T, Cox J. The MaxQuant computational platform for mass spectrometry-based shotgun proteomics. Nat Protoc 2016; 11:2301-19. [PMID: 27809316].

22. Tyanova S, Temu T, Sinitcyn P, Carlson A, Hein MY, Geiger T, Mann M, Cox J. The Perseus computational platform for comprehensive analysis of (prote)omics data. Nat Methods 2016; 13:731-40. [PMID: 27348712].

23. Cehofski LJ, Kruse A, Alsing AN, Sejergaard BF, Nielsen JE, Schlosser A, Sorensen GL, Grauslund J, Honoré B, Vorum H. Proteome Analysis of Aflibercept Intervention in Experimental Central Retinal Vein Occlusion. Molecules 2022; 27:3360-[PMID: 35684299].

24. Cehofski LJ, Kruse A, Magnusdottir SO, Alsing AN, Nielsen JE, Kirkeby S, Honoré B, Vorum H. Dexamethasone intravitreal implant downregulates PDGFR-α and upregulates caveolin-1 in experimental branch retinal vein occlusion. Exp Eye Res 2018; 171:174-82. [PMID: 29505751].

25. Mæng MO, Roshanth N, Kruse A, Nielsen JE, Kjærgaard B, Honoré B, Vorum H, Cehofski LJ. Laser-Induced Porcine Model of Experimental Retinal Vein Occlusion: An Optimized Reproducible Approach. Medicina (Kaunas) 2023; 59:243-[PMID: 36837445].

26. Cehofski LJ, Mandal N, Honoré B, Vorum H. Analytical platforms in vitreoretinal proteomics. Bioanalysis 2014; 6:3051-66. [PMID: 25496257].

27. de Jong S, Gagliardi G, Garanto A, de Breuk A, Lechanteur YTE, Katti S, van den Heuvel LP, Volokhina EB, den Hollander AI. Implications of genetic variation in the complement system in age-related macular degeneration. Prog Retin Eye Res 2021; 84:100952[PMID: 33610747].

28. Armento A, Ueffing M, Clark SJ. The complement system in age-related macular degeneration. Cell Mol Life Sci 2021; 78:4487-505. [PMID: 33751148].

29. Kim BJ, Liu T, Mastellos DC, Lambris JD. Emerging opportunities for C3 inhibition in the eye. Semin Immunol 2022; 59:101633[PMID: 35787973].

30. Kmiecik AM, Dzięgiel P, Podhorska-Okołów M. Nucleobindin-2/Nesfatin-1-A New Cancer Related Molecule? Int J Mol Sci 2021; 22:8313-[PMID: 34361082].

31. Cehofski LJ, Honoré B, Vorum H. A Review: Proteomics in Retinal Artery Occlusion, Retinal Vein Occlusion, Diabetic Retinopathy and Acquired Macular Disorders. Int J Mol Sci 2017; 18:907-[PMID: 28452939].

32. Cavallaro T, Martone RL, Dwork AJ, Schon EA, Herbert J. The retinal pigment epithelium is the unique site of transthyretin synthesis in the rat eye. Invest Ophthalmol Vis Sci 1990; 31:497-501. [PMID: 1690688].

33. Cehofski LJ, Kruse A, Alsing AN, Nielsen JE, Pedersen S, Kirkeby S, Honoré B, Vorum H. Intravitreal bevacizumab upregulates transthyretin in experimental branch retinal vein occlusion. Mol Vis 2018; 24:759-66. [PMID: 30581282].

Articles are provided courtesy of Emory University and The Abraham J. & Phyllis Katz Foundation. The print version of this article was created on 2 July 2024. This reflects all typographical corrections and errata to the article through that date. Details of any changes may be found in the online version of the article.